

Probing Primordial Black Holes with upcoming Radio Telescopes: a case study for LOFAR2.0, FAST Core Array and BINGO

Joao R. L. Santos^{1,2,3,4,*}, Guillem Domènech^{3,5,†} and Amilcar R. Queiroz^{1‡}

¹*Unidade Acadêmica de Física, Universidade Federal de Campina Grande,
Caixa Postal 10071, 58429-900, Campina Grande, Paraíba, Brazil.*

²*Unidade Acadêmica de Matemática, Universidade Federal de Campina Grande,
58429-970, Campina Grande, Paraíba, Brazil.*

³*Institute for Theoretical Physics, Leibniz University Hannover,
Appelstraße 2, 30167 Hannover, Germany.*

⁴*Institut für Theoretische Physik, Ruprecht-Karls-Universität Heidelberg,
Philosophenweg 16, D-69120 Heidelberg, Germany and*

⁵*Max Planck Institute for Gravitational Physics,
Albert Einstein Institute, 30167 Hannover, Germany.*

Fast Radio Bursts (FRBs) are among the most intriguing phenomena observed in radio astronomy. So far, about 130 FRB signals have been confirmed and characterized by different surveys, and the CHIME telescope has recently reported a new catalog of 4539 bursts. Therefore, these numbers are expected to increase in the coming years. The detection, or lack thereof, of lensed FRB events can be used to probe Primordial Black Holes (PBHs) as a fraction of dark matter. We investigate the potential of three upcoming radio telescopes, LOFAR2.0, FAST Core Array, and BINGO, to test the PBH scenario. We forecast that LOFAR2.0 will constrain $f_{\text{PBH}} < 0.16$ for PBH masses $M_{\text{PBH}} > 1 M_{\odot}$, while FAST Core Array and BINGO will restrict $f_{\text{PBH}} < 0.39$ for $M_{\text{PBH}} > 10 M_{\odot}$ and $M_{\text{PBH}} > 10^{-2} M_{\odot}$, respectively. Despite the existence of stricter constraints, FRB lensing offers an independent and complementary probe of PBHs in the Universe, which will improve in the future.

I. INTRODUCTION

FRB observations have attracted significant attention in the astronomy and physics communities since the first reported detection in 2007 of a bright, unidentified radio signal in the 1.4 GHz survey of the Magellanic Cloud conducted by the Parkes radio telescope [1]. After that, around a thousand possible candidates have been reported, and, at the time of writing,¹ 131 FRBs have been confirmed by multiple surveys [2] and a recent catalog with 4539 bursts was reported by CHIME (Canadian Hydrogen Intensity Mapping Experiment) telescope [3].

The flux densities and luminosities of the FRBs are high, varying between 0.5 - 100 Jy, and $\sim 10^{36} - 10^{44}$ erg s⁻¹ [4], and of short time durations, usually around ms - μ s. The short time window poses an experimental challenge, namely how to determine an optimal backend resolution for measuring these bursts. The events are mainly extragalactic and usually unique. The fact that we are observing mainly single bursts makes it difficult to understand the origin of such phenomena.

The leading explanation is that FRBs come from neutron stars, specially magnetars [5–8], although there are alternative explanations involving Primordial Black Holes (PBHs) swallowing neutron stars [9–13] and the merger of charged PBHs [14, 15]. Moreover, another interesting

* joorafael@df.ufcg.edu.br

† guillem.domenech@itp.uni-hannover.de

‡ amilcarq@df.ufcg.edu.br

¹ Data obtained from the Transient Name Server: <https://www.wis-tns.org/>

question is whether repeating and non-repeating FRBs represent distinct classes of objects [5].

The time delay of the FRB signal across different radio frequency channels depends on the interaction of free electrons along the signal’s path. Higher-wavelength fronts arrive later than shorter ones. This effect is parametrized by the so-called dispersion measure (DM). From the DM, one can estimate the FRB’s redshift and characterize the matter along the line of sight. As most of the detected FRBs are extragalactic in origin, they may also be used to constrain cosmological models [16], estimate the fraction of baryonic mass in the intergalactic medium (IGM) [17–19], and to measure the Hubble parameter [16].

Observations of FBRs by the new generation of radio telescopes may be a promising path for investigating and characterizing the abundance of compact dark matter objects, like PBHs, as pioneered by Muñoz et al. [20]. Since then, several investigations have been published in the literature over the last few years, as we can see, for instance, in [21–25]. In particular, the CHIME Collaboration constrained the fraction of PBHs as dark matter to $f_{\text{PBH}} < 0.8$ for $M \sim 10^{-3} M_{\odot}$ [23]. For studies investigating the impact of modifications of gravity, and different mass functions and FRB distributions see Refs. [24] and [26], respectively.

PBHs may form by the collapse of large fluctuations in the primordial plasma, as first pointed out by Zel’dovich and Novikov [27] and Hawking and Carr [28, 29]. Depending on their mass, PBHs may explain all the dark matter [30], the OGLE and HSC microlensing candidate events [31–33], some of the LIGO/Virgo/KAGRA GW events [34, 35] and the seeds of supermassive black holes [36–38]. For recent reviews on PBHs see Refs. [13, 39–42]. In the mass range of our interest, that is $M > 10^{-3} M_{\odot}$, the PBH fraction is currently constrained by lensing of SN type Ia [43], microlensing of stars in the Magellanic Clouds [44, 45], caustic crossings [46], LVK binary black hole mergers [47] and the Cosmic Microwave Background (CMB) [48, 49]. Current constraints range from $f_{\text{PBH}} < 10^{-2}$ for sub-solar mass PBHs down to $f_{\text{PBH}} < 10^{-8}$ for intermediate mass PBHs. For a detailed summary of constraints see Refs. [25, 50, 51]. Nevertheless, it is important to stress that FRB lensing offers an independent and complementary way to probe PBHs in these mass ranges, and that these test will improve in the future.

In this work, we investigate the potential to probe PBHs with the radio telescopes LOFAR (LOW Frequency ARray) and FAST (Five-hundred-meter Aperture Spherical radio Telescope), which are undergoing upgrades, and BINGO (Baryon Acoustic Oscillations from Integrated Neutron Gas Observations), which is under construction in Brazil. The upgrade to LOFAR, called LOFAR2.0 [52, 53], aims to double its observing speed and expand its angular resolution [54]. The FAST Core Array upgrade will image FRBs and pulsars with much greater detail, enabling better characterization and revealing their origins and evolution [55]. These upgrades are expected to be completed by 2026 and 2030, respectively.

BINGO will be one of the first fixed transit telescopes dedicated to exploring BAO at this frequency band [56]. In addition to the main radio telescope, there will be a series of auxiliary radio telescopes, forming an interferometric array that will not only enhance the quality of BAO data measurements but also enable BINGO to become an excellent machine for measuring transient radio phenomena such as pulsars and FRBs [57]. BINGO is in its final stages of construction, and it is expected to start operating in the coming years. BINGO is also planning a joint operation together with FAST, Tianlai, ASTRON, and Nançay Observatory, in a phase called BINGO/ABDUS (Advanced Bingo Dark Universe Studies) [58]. The BINGO/ABDUS collaboration intends to increase the redshift range of BINGO, observing radio signals from $z \sim 2.1$, and covering a larger

fraction of the sky in a resolution between $27' - 40'$ [58]. Thus, LOFAR, FAST, and BINGO will increase the number of FRB detections in the coming years and support the characterization of FRBs detected by other surveys, such as CHIME.

To derive the forecasts, we apply the work of Muñoz et al. [20] and study the impact of the signal-to-noise (SNR) ratio, the total number of measured bursts, and the time resolution of these different radio telescopes in the computation of the optical depth and of the fraction of PBHs. Furthermore, our forecast is based on the most recent catalog of 131 FRBs recently provided by Jia et al. [2] and detailed in App. A.

This work is organized as follows. In Section II, we review generalities on FRB lensing as probes of PBHs. In section III, we present the details about each radio telescope, our forecast for the optical depth and for the fraction of PBHs, and a summary of our results. Section IV is dedicated to our conclusions and discussion. Throughout this work, we use the following constants and parameters in our numerical calculations: $c = 299,792,458$ m/s, $G = 6.67430 \times 10^{-11}$ m³ kg⁻¹ s⁻², $M_{\odot} = 1.98847 \times 10^{30}$ kg, $H_0 = 67.7$ km s⁻¹ Mpc⁻¹. When needed, we use the cosmological parameters from the best fit of Planck 2018 [59], that is $\Omega_M = 0.30966$, $\Omega_{\Lambda} = 0.68884$, $\Omega_b = 0.04897$, and $\Omega_c = 0.26069$. Ω_M , Ω_b , Ω_c and Ω_{Λ} are the density fraction of matter, baryons, dark matter and dark energy in the Universe, respectively.

II. REVIEW ON FRBS LENSING

In this section we present the generalities of FRBs characterization, gravitational lensing by a point source and the optical depth of a survey.

A. FRBs characterization

One of the most challenging parameters to identify using FRBs' data is the redshift of each source, which can be estimated from the DM. The calculation of DM typically involves various contributions, primarily due to the host galaxy, the intergalactic medium, and the Milky Way's interstellar medium. The observed DM is computed by [60]

$$DM_{\text{obs}}(z) = DM_{\text{MW}} + DM_{\text{IGM}} + \frac{DM_{\text{host}}}{1+z}, \quad (2.1)$$

where $DM_{\text{MW}} = DM_{\text{MW,ISM}} + DM_{\text{MW,halo}}$ is the dispersion measure of the Milky Way, with $DM_{\text{MW,ISM}}$ as the galactic interstellar medium ($\sim 10^0 - 10^3$ pc cm⁻³) and $DM_{\text{MW,halo}}$ the galactic halo contributions, respectively. The Milky Way halo contribution $DM_{\text{MW,halo}}$ is constrained by different surveys as lying between $50 - 117$ pc cm⁻³ [23, 61]. Furthermore, the dispersion measure related to the intergalactic medium, DM_{IGM} varies between ($\sim 10^2 - 10^3$ pc cm⁻³), while the one corresponding to the host galaxy DM_{host} covers the range ($\sim 10^0 - 10^3$ pc cm⁻³). Note that the factor $(1+z)$ in (2.1) is due to cosmic expansion.

The dispersion measure DM_{IGM} is determined using the Macquart relation [62], whose explicit form is

$$DM_{\text{IGM}}(z) = A \Omega_b H_0^2 \int_0^z \frac{(1+z) x_e(z)}{H_0 \sqrt{\Omega_M (1+z)^3 + \Omega_{\Lambda}}} dz; \quad A = \frac{3c f_{\text{IGM}}}{8\pi G m_p}, \quad (2.2)$$

where $f_{\text{IGM}} = 0.83$ is the baryon mass fraction in the IGM [63], H_0 is the Hubble parameter today, and m_p is the proton mass. Lastly, in Eq. (2.2), $x_e(z)$ denotes the free electron fraction (or degree of plasma ionization), which is given by

$$x_e(z) = Y_{\text{H}}x_{e,\text{H}}(z) + \frac{1}{2}Y_{\text{He}}x_{e,\text{He}}(z), \quad (2.3)$$

where $Y_{\text{H}} = 3/4$, $Y_{\text{He}} = 1/4$, $x_{e,\text{H}}(z)$ and $x_{e,\text{He}}(z)$ are the mass fractions and the ionization fractions of hydrogen and helium, respectively. In our analysis, we consider $x_{e,\text{H}}(z) = x_{e,\text{He}}(z) = 1$ since hydrogen and helium are fully ionized at $z < 3$ [64, 65], yielding $x_e = 7/8$. The previous relations are used to estimate the redshift of the source for different FRB pulses, which are presented together with the values of DM_{obs} and DM_{MW} in App. A.

B. Gravitational lensing by a point source

To characterize lensing effects due to PBHs, we treat of them as a point lens, with the standard angular Einstein radius given by [20, 66]

$$\theta_E = 2 \sqrt{\frac{G M_L}{c^2} \frac{D_{LS}}{D_S D_L}}, \quad (2.4)$$

where D_S , D_L and D_{LS} are the distances to the source, to the lens and between the source and the lens, respectively. The deflection angle, the normalized impact parameter y , and the angular impact parameter β are defined as

$$\alpha = \frac{\theta_E^2}{\theta}; \quad y = \frac{\beta}{\theta_E}; \quad \beta = \theta - \frac{\theta_E^2}{\theta}. \quad (2.5)$$

A point lens will produce two images located at

$$\theta_{\pm} = \left(\frac{\beta}{2} \pm \frac{1}{2} \sqrt{\beta^2 + 4\theta_E^2} \right). \quad (2.6)$$

For the magnification ratio we adopt the approach of Kalita et al. [24], which yields

$$\mu = \left(\frac{y + \sqrt{y^2 + 4}}{y - \sqrt{y^2 + 4}} \right)^2, \quad (2.7)$$

enabling us to constrain y_{max} as

$$y_{\text{max}} = \frac{q - 1}{\sqrt{q}}; \quad q = \sqrt{\mu_{\text{max}}}. \quad (2.8)$$

The maximum value of the magnification ratio is defined as that with $\mu_{\text{max}} = 1/3 \text{ SNR}$, where SNR depends on the radio telescope. The factor 1/3 corresponds to a realistic threshold for the signal-to-noise ratio at which the burst can be detected in autocorrelation [23, 67]. For such a threshold, the signal can be distinguished from noise fluctuations [24]. Therefore, this parameter depends directly on the design of the instruments considered in this forecast. Note that Eq. (2.8) circumvents the need to set a threshold value for the flux ratio in the computation of y_{max} , yielding a more realistic assumption on the forecast.

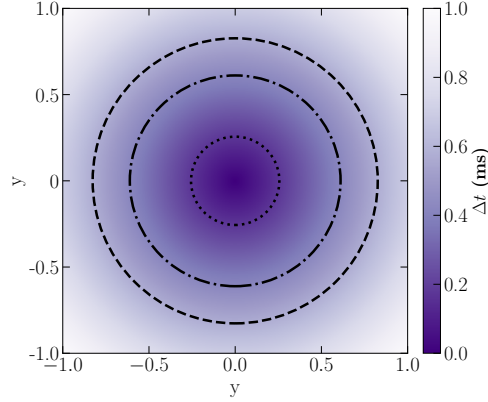


FIG. 1: Lens plane to characterize the detectability of Δt with different SNR. The figure was depicted considering $z_L = 0$, $M_L = M_\odot$, SNR = 5 (dotted annulus), SNR = 10 (dashed-dotted annulus), SNR = 15 (dashed annulus), and Δt variations are scaled in ms.

The presence of a standard Schwarzschild lens will result in a time delay between the images, given by [20, 66]

$$\Delta t = (1 + z_L) \frac{D_\Delta \theta_E^2}{c} \left[\frac{y}{2} \sqrt{y^2 + 4} + \ln \left(\frac{\sqrt{y^2 + 4} + y}{\sqrt{y^2 + 4} - y} \right) \right], \quad (2.9)$$

where z_L is the redshift of the lens and $D_\Delta = D_L D_S / D_{LS}$. We illustrate the features of the time delay in Fig. 1, considering $z_L = 0$, $M_L = M_\odot$, SNR = 5 (dotted annulus), SNR = 10 (dashed-dotted annulus), SNR = 15 (dashed annulus). Δt variations are scaled in ms. From Fig. 1, we see that larger SNR allow the radio telescopes to observe larger values of time delay, corresponding to an increase in the maximum values of y . As we will reveal in the forecast results, the SNR will be crucial for setting bounds on the maximum mass fraction of PBHs.

C. Event rate and optical depth

Let us now compute the probability of a FRB located at a redshift z_S to be lensed. The optical depth of this radio transient reads [20]

$$\tau(M_L, z) = \int_0^z d\chi(z_L) (1 + z_L)^2 n_L \sigma(M_L, z_L), \quad (2.10)$$

where

$$\chi(z) = c \int_0^z \frac{dz}{H(z)}, \quad H(z) = H_0 \sqrt{\Omega_M (1+z)^3 + \Omega_\Lambda}, \quad (2.11)$$

which are the comoving distance and the Hubble function, respectively. Moreover, n_L is the comoving number density of lenses and

$$\sigma(M_L, z_L) = \frac{4\pi G M_L}{c^2} \frac{D_L D_{LS}}{D_S} (y_{\max}^2(\mu) - y_{\min}^2(M_L, z_L)), \quad (2.12)$$

is the lensing cross-section of a point lens with mass M_L .

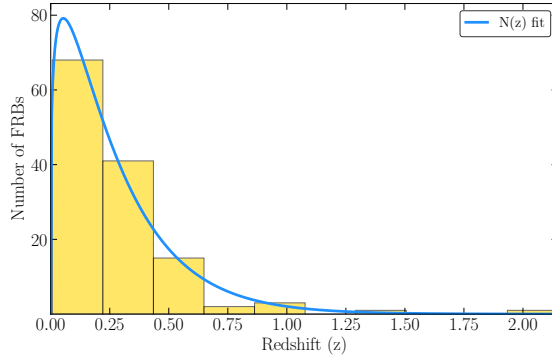


FIG. 2: Histogram of the recent data of 131 confirmed FRB events. The fit (2.16) is shown with the solid blue line. The dataset used is presented in App. A.

For simplicity, let us assume a monochromatic mass function with a peak at M_L . In that case, one has that

$$\frac{dn_L}{dM} = \frac{\rho_0}{M_L} f_{\text{PBH}} \Omega_c \delta(M - M_L); \quad n_L = \frac{\rho_0 f_{\text{PBH}} \Omega_c}{M_L}, \quad (2.13)$$

where f_{PBH} is the fraction of PBHs as dark matter and $\rho_0 = 3H_0^2/8\pi G$ is the critical density of the Universe. Substituting Eqs. (2.12) and (2.13) into Eq. (2.10) we rewrite the lensing optical depth as

$$\tau(M_L, z) = \frac{3}{2} f_{\text{PBH}} \Omega_c \int_0^z dz_L \frac{H_0^2}{cH(z_L)} \frac{D_L D_{LS}}{D_S} (1 + z_L)^2 (y_{\text{max}}^2(\mu) - y_{\text{min}}^2(M_L, z_L)), \quad (2.14)$$

where y_{min} is obtained by solving Eq. (2.9) for Δt_{min} . The values used for Δt_{min} depend on the better time resolution of each radio telescope considered in this forecast.

The integrated optical depth is given by

$$\bar{\tau}(M_L) = \int dz \tau(M_L, z) N(z), \quad (2.15)$$

where $N(z)$ is a distribution function. Since the number of cataloged FRB is smaller than 10^4 , which would be the ideal amount of events to properly constrain a lensing forecast [20], we fit the present FRB dataset with an analytic distribution. In App. A, we present the most recent data of 131 confirmed FRB pulses, which were used to build the histogram illustrated in Fig. 2. The tables in App. A represent a combination of two datasets previously used by references [68] and [2] to constrain Hubble and cosmographic parameters.

We find that a fit to $N(z)$ in the histogram of Fig. 2 is given by a Gamma distribution, whose explicit form is

$$N(z) = N_0 z^{a_1} e^{-a_2 z}; \quad N_0 = 208.7210; \quad a_1 = 0.2465; \quad a_2 = 4.6269. \quad (2.16)$$

To reach this fit, we tested three different distributions: the Lognormal, Gamma, and Weibull. The tests consisted of computing the log-likelihood of the redshift data and evaluating how well each distribution fits the data. Then, we applied the Akaike Information Criterion (AIC) to find the distribution corresponding to the minimal value of this criterion. Such a procedure enabled us to determine the non-Gaussian distribution introduced in Eq. (2.16). Note that, although the analytical fit may improve in the future, we do not expect our results to change substantially.

Telescope	SNR	Best time resolution	Max number of FRBs	Reference
LOFAR2.0	7	$5.12 \mu\text{s} - 983 \mu\text{s}$	4500	[69, 70]
FAST Core Array	10	$270 \mu\text{s} - 128 \text{ms}$	900	[58, 71]
BINGO	10	$1 \mu\text{s} - 1 \text{ms}$	900	[56–58, 72]

TABLE I: Design features of the three radio telescopes considered in the forecast, and the estimated maximum number of FRBs that each radio telescope could measure in the near future.

III. FORECASTS FOR UPCOMING RADIO TELESCOPES

Before presenting the results of our forecast, let us briefly introduce each of the radio telescopes considered here and justify the parameters chosen as our constraints.

A. The LOFAR, FAST and BINGO radio telescopes

We summarize the design features of each radio telescope implemented in the numerical integrations in Table I, which we use to determine the optical depth and bounds on the fraction of PBHs. The public data employed is reported in Refs. [56–58, 69–72]. We describe below each radio telescope separately.

i) **LOFAR** is a radio telescope based in the north of the Netherlands that started its operations in 2012. The telescope consists of an array of omnidirectional antennas forming sets of stations, and was originally designed to explore a frequency range between 10 – 240 MHz. In addition to its main site, LOFAR has 51 stations across the Netherlands, Germany, France, the United Kingdom, Ireland, and Sweden. The main scientific motivation for its construction was to explore 21 cm signals from the reionization, covering $z = 6 - 20$, and from the Cosmic Dawn ($z = 20 - 50$). As secondary objectives, LOFAR’s design is also suitable for detecting signals from ultra-high-energy cosmic rays, conducting surveys of pulsars and radio transients, searching for high-redshift radio sources, and detecting FRBs [69].

In respect to the detection of FRBs, LOFAR has proven to be a great machine for characterizing these transient phenomena, covering the 150 MHz activity frequency band of 14 repeating FRBs measured by LOFAR and CHIME radio telescopes [70]. The data were cataloged between 2012 and 2020 from the so-called LOTAAS (LOFAR Tied-Array All-Sky Survey) [73], with a frequency resolution of 48.8 kHz and a time resolution of 0.983 ms.

In the next few years, LOFAR will be fully upgraded to LOFAR2.0, increasing its computational capacity and resolution, allowing it to search for FRBs over hundreds of tied-array beams. After such an update, the telescope expects to detect 0.3 – 9 FRBs per week with $\text{SNR} = 7$, and with possible nanosecond time resolution [74], covering the redshift interval $1 < z < 3$. The actual minimal time resolution of the radio telescope is $5.12 \mu\text{s}$ [69], which is one of the constraints used in our forecast, as can be seen in Table I.

ii) **FAST** is the largest single-dish radio telescope in operation worldwide. It was completed in 2016 and operates in a frequency range between 70 MHz – 3 GHz. FAST also has an ultra-wideband receiver operating between 270 – 1620 MHz and 19 dual-polarized beams working in the frequency range of 1050 – 1450 MHz. The main scientific objectives of the FAST telescope are to conduct

a large-scale neutral hydrogen survey, observe pulsars and timing arrays, and detect interstellar molecules.

FAST was not initially designed to detect FRBs. In fact, its relatively small field of view makes the observation of such transients challenging compared with surveys fully dedicated to FRBs, such as the CHIME radio telescope. Nevertheless, FAST has extremely high sensitivity (more than twice that of the Arecibo radio telescope), and it can be useful for characterizing pulsars and FRBs by improving the accuracy of their positioning and detecting the high-precision neutral hydrogen absorption line generated by these transients in real time. FAST detects fast radio bursts using its real-time FRB searching system, which recently was able to characterize pulses with a dispersion measure range of $20 - 1000 \text{ pc cm}^{-3}$, a frequency resolution of 122.07 kHz , SNR equals to 10, and time resolution between $128 \text{ ms} - 270.336 \mu\text{s}$ [71]. Some of these parameters are presented in Table I, and were considered in our forecast.

In the next few years, FAST will be upgraded with the construction of the so-called FAST Core Array [55]. This new array will consist in 24 secondary antennas with 40 m diameter, installed in a radius of 5 km from the FAST radio telescope. This new array will increase the resolution and the sensitivity of FAST, allowing it to localize transient bursts, which may unveil new insights about the sources of FRBs.

iii) **BINGO** is a radio telescope in its final phase of construction at the city of Aguiar, located in the Northeast of Brazil. BINGO will be a single-dish telescope with a 40 m primary mirror, and an array of 28 horns (receivers). The main objective of the project is to observe the 21 cm line associated with the hyperfine emission of the hydrogen atom. The horns are designed to operate in an optimized range between $980 - 1260 \text{ MHz}$, corresponding to $z = 0.13 - 0.48$. The radio telescope will cover approximately $5,324$ square degrees of the sky over a 5-year observation cycle [56, 58]. BINGO will be part of a new generation of radio telescopes dedicated to investigating the dark sector in a redshift range much closer to the present. Moreover, it represents one of the most relevant experiments developed and operated in Brazil.

Beyond BAO signals, BINGO also aims to be an interesting machine for detecting and localizing FRBs. To do so, it needs to be improved with a set of auxiliary radio telescopes (outriggers) and with a complementary digital backend setup covering a time resolution between $1 \mu\text{s} - 1 \text{ ms}$. The expected SNRs vary between $5 - 15$ and this interferometric array forecasts the detection of approximately 70 events per year [57]. The number of detections can be increased to 900 events by considering a joint collaboration between BINGO, ASTRON, Nançay Observatory, FAST, and Tianlai radio telescopes, in a phase named BINGO-ABDUS (Advanced BINGO Dark Universe Studies) [58]. These values were used as thresholds for our forecast of the fraction of PBHs, and are shown in Table I.

B. Forecasts for PBH constraints

We use the values given in Tab. I to forecast the expected constraints on the PBH abundance. In our numerical analysis, we set a minimum and maximum value for the PBH mass given by $M_{\min} = 10^{-2} M_{\odot}$ and $M_{\max} = 3 \times 10^4 M_{\odot}$ respectively [23]. The lower limit, M_{\min} , is set by the highest time resolution of LOFAR of roughly $1 \mu\text{s}$. Smaller lens masses lead to a too short time delay. The upper limit, M_{\max} , is set for convenience. For $M_{\max} > 10^4 M_{\odot}$, there are extremely strong constraints on f_{PBH} from CMB spectral distortions [38, 75]. We used 90 and 131 points for

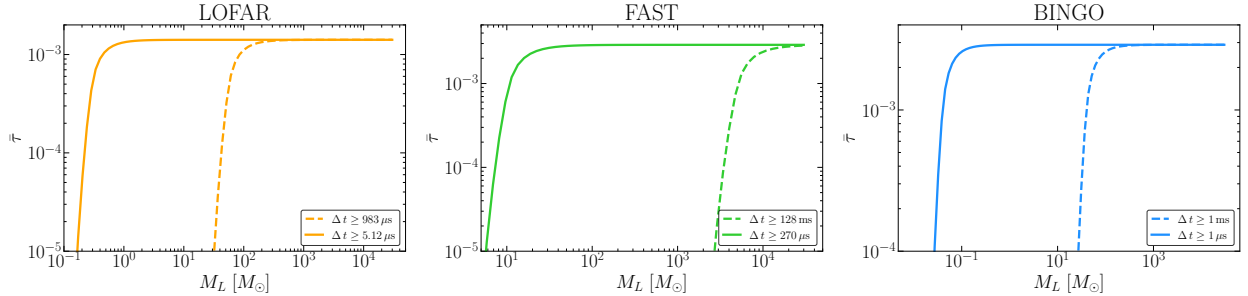


FIG. 3: Total optical depth for LOFAR, FAST, and BINGO. In these graphics, we consider the best time resolution constraints for each radio telescope and $f_{\text{PBH}} = 1$. The solid and dashed lines respectively correspond to the lowest and highest best time resolution in Tab. I.

The asymptotic values are $\bar{\tau} \sim 0.0014$ for LOFAR, and $\bar{\tau} \sim 0.003$ for BINGO and FAST.

integrating over the mass and the redshift grids, respectively.

Now, given a distribution of FRBs, we can compute the integrated optical depths (2.15). We present their main features in Fig. 3. There, we observe that the integrated optical depths grow monotonically as the mass of the lenses increases, as found by Muñoz et al. [20]. The asymptotic values of the optical depths constrain that we expect ~ 6 lensing events detected by LOFAR with masses starting at $M_{\text{PBH}} \sim 1 M_{\odot}$ for $N_{\text{FRB}} = 4500$. For FAST and BINGO, we estimate ~ 3 lensing events detected for $N_{\text{FRB}} = 900$, with PBH masses larger than $M_{\text{PBH}} \sim 30 M_{\odot}$ and $M_{\text{PBH}} \sim 0.2 M_{\odot}$, respectively. From Fig. 3, we also see the influence of time resolution on the bounds of the mass ratios that can be detected by the three telescopes in this forecast. Namely, the higher the time resolution, the lower the mass of the lens that can be resolved.

To find the constraints on the fraction of PBHs considering a null-detection, we work in the optically thin regime approximation, where the probability of a FRB being lensed is $P_{\text{lens}} = 1 - e^{-\bar{\tau}} \approx \bar{\tau}$. In that case, the maximum allowed PBH fraction is

$$f_{\text{PBH max}}(M_{\text{PBH}}) = (N_{\text{FRB}} \bar{\tau}(M_{\text{PBH}}))^{-1}, \quad (3.1)$$

where from now on we will set the lens mass to be the PBH mass, namely $M_L = M_{\text{PBH}}$. We also impose that $f_{\text{PBH max}} \leq 1$ for consistency. We show the forecast for $f_{\text{PBH max}}$ versus M_{PBH} in Fig. 4. In the shaded regions of Fig. 4, we present the exclusion regions for $f_{\text{PBH max}}$ for each radio telescope. The shaded colored regions unveil the lowest best interval of time resolution of LOFAR (orange), FAST (green), and BINGO (blue), to compute f_{PBH} . The shaded gray regions mark the constraints use the highest best interval of time resolution of Tab. I, also see Fig. 3.

From the left panel of Fig. 4, we see that the upgrades of LOFAR could constrain a maximum fraction of $f_{\text{PBH}} < 0.16$ for $M_{\text{PBH}} \sim 1 - 10^2 M_{\odot}$. For the next upgraded version of FAST operating together with the BINGO-ABDUS consortium, we would have the possibility of constraining a maximum fraction of $f_{\text{PBH}} < 0.39$ for $M_{\text{PBH}} \sim 10^2 - 10^4 M_{\odot}$. Note that, since the time resolution reported by FAST is $128 \text{ ms} - 270 \mu\text{s}$, it can only provide constraints for lenses with high masses. In the case of BINGO-ABDUS, the collaboration aims to achieve a $\text{SNR} = 10$ (in a more conservative scenario) and a time resolution of between μs and ms . Therefore, BINGO-ABDUS would be able to constrain a maximum fraction of $f_{\text{PBH}} < 0.39$, the same as FAST, but with a higher time resolution, extending the constraint to lower masses and covering an optimistic range between $10^{-1} M_{\odot}$ and $10^2 M_{\odot}$.

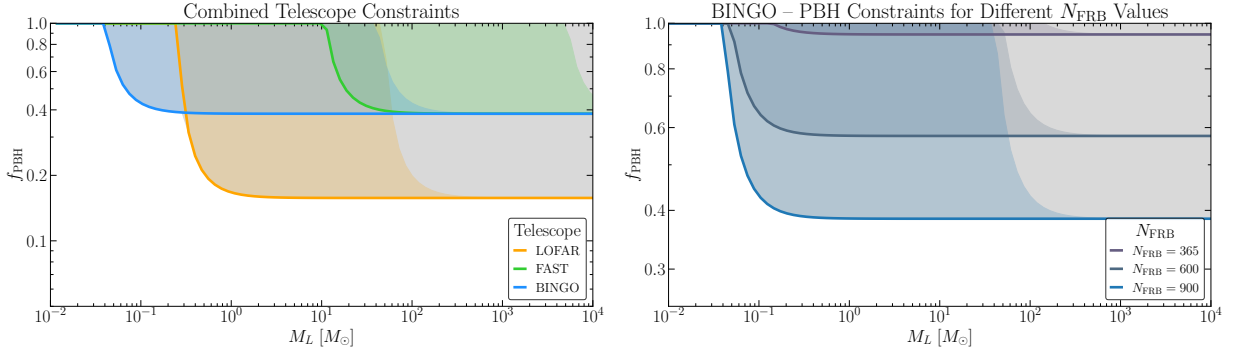


FIG. 4: Forecast for the fraction of primordial black holes allowed as point lenses. **Left:** The colored shaded regions represent the best constraints of exclusion for LOFAR (orange), FAST (green), and BINGO (blue) using the lowest best time resolution of Tab. I. The gray shaded regions correspond to the highest best time resolution of Tab. I, instead. **Right:** Forecast for the fraction of primordial black holes for BINGO, considering $N_{\text{FRB}} = 350$ (purple), $N_{\text{FRB}} = 600$ (darker blue), and $N_{\text{FRB}} = 900$ (lighter blue). The colored shade regions represent the best constraints for f_{PBH} considering a time resolution between $1 \mu\text{s} - 1 \text{ms}$.

In the right panel of Fig. 4, we show a forecast for BINGO varying the detected number of FRB events, namely $N_{\text{FRB}} = 350$ (purple), $N_{\text{FRB}} = 600$ (darker blue), and $N_{\text{FRB}} = 900$ (lighter blue). We find that BINGO needs to detect more than 350 FRBs to be a competitive radio telescope for constraining f_{PBH} . As we see from Fig. 4, if $N_{\text{FRB}} = 350$, we find that $f_{\text{PBH}} < 0.95$ for $M_{\text{PBH}} > 1 M_{\odot}$. For $N_{\text{FRB}} = 600$, the bound goes down to $f_{\text{PBH}} < 0.58$ for $M_{\text{PBH}} > 10^{-1} M_{\odot}$. For $N_{\text{FRB}} = 900$, which is approximately the maximum number of expected events, we recover the results of the left hand side of Fig. 4. We see that, for BINGO’s resolution, a larger number of FRBs impacts not only the bounds on f_{PBH} , but also the range of M_{PBH} .

To compare our forecast with current observational constraints on PBHs, we generated Fig. 5. There we can observe bounds generated by FRB/CHIME [23], SNe [43], Icarus [46], OGLE [44, 76], Substellar mergers [77], LIGO/VIRGO/KAGRA [40, 47], and CMB [48]. These bounds cover a broad range of PBHs’ masses, here highlighted from $10^{-4} - 10^4 M_{\odot}$. They can also constrain fractions of PBHs $< 10^{-3}$, as we can see from the bounds provided by OGLE and CMB. By comparing our forecast with these bounds, we find it is compatible with forecasts for FRBs and Supernovae reported so far. We also realize that the three radio telescopes can contribute to different surveys in a new and independent way. Moreover, the precision of this forecast can be enhanced as new FRBs are reported and characterized in the near future with better instrumental resolution.

IV. CONCLUSIONS AND DISCUSSION

In the next years, the radio telescopes LOFAR, FAST, and BINGO are expected to detect of the order of 1000 FRB events (see Tab. I). A null-detection of FRB lensed events will constrain the fraction of PBHs as dark matter, $f_{\text{PBH}} \lesssim \mathcal{O}(0.1)$. More concretely, we showed that LOFAR2.0 is expected to yield $f_{\text{PBH}} < 0.16$ for $M_{\text{PBH}} > 0.1 M_{\odot}$, while FAST Core Array together with BINGO (in the BINGO-ABDUS joint phase [58]) should constrain $f_{\text{PBH}} < 0.38$ for $M_{\text{PBH}} > 0.01 M_{\odot}$. While these forecasts are not yet competitive with current constraints—in our same PBH mass

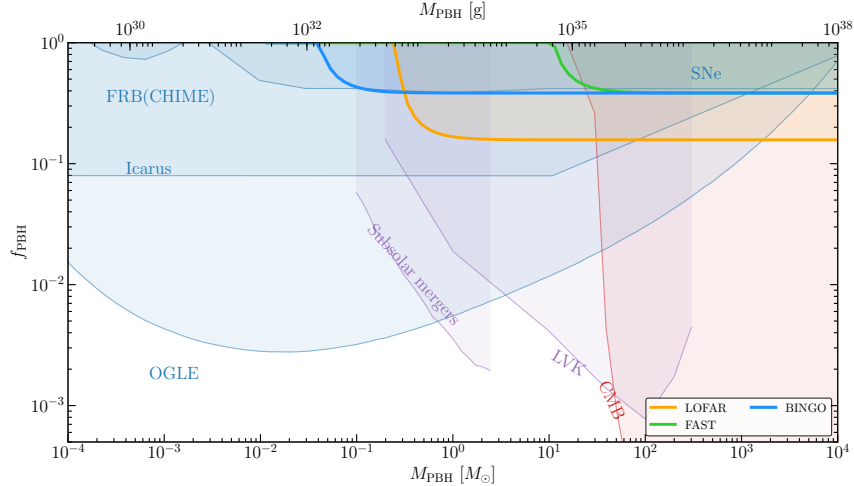


FIG. 5: Constraints on the fraction of primordial black holes from different surveys combined with our forecast. The colored shaded regions represent the best constraints of exclusion provided by FRB lensing using CHIME [23] (dark blue), SN lensing [43] (dark blue), Icarus caustic-crossing [46] (blue), OGLE [78] (light blue), Subsolar mergers [77] (purple), LIGO/VIRGO/KAGRA mergers [79] (light purple), CMB [48] (red), see also [49]. We used the public code PBHBOUNDS [40, 80] to plot existing constraints. The forecasts derived in this work are LOFAR (highlighted orange), FAST (highlighted green), and BINGO (highlighted blue). For the telescope constraints, we consider the lowest-best time resolution in Tab. I.

range microlensing of stars yields $f_{\text{PBH}} < 0.01$ for $0.01 M_{\odot} < M_{\text{PBH}} < 100 M_{\odot}$, and CMB bounds $f_{\text{PBH}} < 10^{-8}$ for $M_{\text{PBH}} > 100 M_{\odot}$ [25, 50, 51]–, FRB lensing is a new and independent way to test the PBH scenario, which will improve in the future. For instance, we find that reaching $N_{\text{FRB}} = 2 \times 10^4$ and $N_{\text{FRB}} = 2 \times 10^5$ would yield $f_{\text{PBH}} < 10^{-2}$ and $f_{\text{PBH}} < 10^{-3}$ respectively, in agreement with Ref. [20]. We show our forecasts together with existing constraints in Fig. 5.

Note that, although our results build upon the work of Ref. [20], the new aspect of our work is the use concrete design features of upcoming radio telescopes. We hope that our forecast may be useful for the operation of these radio telescopes in the near future, shaping possible interesting applications for their upcoming FRB data. Furthermore, the methodology we adopted in our work can be applied to other surveys [23] to include other types of gravitational lenses, dispersion effects such as plasma screens [23, 24], and test gravitational theories [24].

Lastly, in deriving our forecasts, we have assumed a monochromatic PBH mass function for simplicity. Considering a broad mass function will not qualitatively change the constraints on the magnitude of f_{PBH} but may change the PBH mass range probed depending on the mass function width. Furthermore, we have not considered possible decoherence effects from the interaction of FRBs with the intervening intergalactic medium. These effects mainly deteriorate the constraining power of FRB lensing in the large mass lens regime [23]. Our forecasts of Fig. 4 can be understood as the best case scenario for the radio telescopes considered. We leave a more detailed analysis for future work when new data becomes available.

ACKNOWLEDGMENTS

JRLS acknowledges support from CNPq (Grants 309494/2021-4 and 302190/2025-2), FAPESQ-PB (Grant 1356/2024), CAPES Finance Code 001, and Alexander von Humboldt-Stiftung Foundation. JRLS also acknowledges the hospitality of the ITP at Leibniz University Hannover, and the ITP and ITA at the University of Heidelberg, where this work was built. A.R.Q. acknowledges FAPESQ-PB, and the support by CNPq under process number 310533/2022-8. G.D acknowledges support from the DFG under the Emmy-Noether program (project number 496592360) and the JSPS KAKENHI grant No. JP24K00624.

Appendix A: Fast radio bursts dataset

In this appendix we list the FRBs used in our forecast. We include FRB names, redshift, DM and reference of origin in Tabs. II and II.

FRB (name)	Redshift z	DM_{obs} (pc cm ⁻³)	DM_{MW} (pc cm ⁻³)	Ref.	FRB (name)	Redshift z	DM_{obs} (pc cm ⁻³)	DM_{MW} (pc cm ⁻³)	Ref.
20250316A	0.0067	161.82	70	[81]	20241228A	0.1614	246.53	23.8	[104]
20171020A	0.00867	114.1	38	[82]	20210603A	0.177	500.15	40	[105]
20220319D	0.011228	110.98	133.3	[83]	20220529A	0.1839	246.0	39.93	[106, 107]
20231229A	0.0190	198.5	58.2	[84, 85]	20230311A	0.1918	364.3	67.24	[84, 108]
20240210A	0.0237	283.75	31	[86]	20220725A	0.1926	290.4	31	[86]
20181220A	0.0275	209.4	126	[87, 88]	20121102A	0.19273	551.92	200	[92, 109]
20231230A	0.0298	131.4	61.58	[84, 89]	20221106A	0.2044	343.8	35	[86]
20200120E	0.03	87.82	30	[90]	20240215A	0.21	549.5	48.0	[100]
20181030A	0.03	103.5	30	[88, 91]	20230730A	0.2115	312.5	85.16	[84]
20181223C	0.03024	112.5	20	[87]	20210117A	0.214	729.0	34.0	[110]
20190425A	0.03122	128.2	49	[87, 88]	20221027A	0.229	452.5	47.2	[100]
20180916B	0.0337	348.76	200	[88, 92]	20191001A	0.234	506.92	44.0	[92, 111]
20230718A	0.035	477	393	[93]	20190714A	0.2365	504.13	38	[92, 112, 113]
20240201A	0.0427	374.5	38	[86]	20221101B	0.2395	490.7	131.2	[99, 100, 114]
20220207C	0.0430	262.38	79.3	[83]	20220825A	0.2414	651.24	79.7	[83]
20211127I	0.0469	234.83	42	[92]	20190520B	0.2418	1204.7	60.2	[92, 115]
20201123A	0.0507	433.55	251.93	[94]	20191228A	0.2432	297.5	33	[116]
20230926A	0.0553	222.8	52.62	[84]	20231017A	0.2450	344.2	64.55	[84]
20200223B	0.06024	201.8	45.6	[88, 95]	20220307B	0.2481	499.15	128.25	[83, 117]
20190303A	0.064	222.4	26	[88, 96]	20221113A	0.2505	411.4	91.7	[99, 100, 114]
20231204A	0.0644	221.0	29.73	[84]	20220831A	0.262	1146.25	126.7	[100]
20231206A	0.0659	457.75	90.46	[84, 97]	20231123B	0.2625	396.7	40.2	[99, 100, 114]
20210405I	0.066	565.17	516.1	[98]	20230307A	0.2710	608.9	37.6	[99, 100, 114]
20180814	0.068	189.4	87	[88, 96]	20221116A	0.2764	640.6	132.3	[99, 100]
20231120A	0.07	438.9	43.8	[99, 100]	20220105A	0.2785	580	21.9	[92, 100]
20231005A	0.0713	189.4	33.37	[84]	20210320C	0.2797	384.59	39.2	[92, 100]
20190418A	0.07132	184.5	71	[87, 88]	20221012A	0.2840	442.20	54.4	[83, 100]
20211212A	0.0715	109	42	[92, 101]	20240229A	0.287	491.15	37.9	[100]
20231123A	0.0729	302.1	90	[84, 101]	20190102C	0.2912	364.55	57.4	[92, 100]
20220912A	0.0771	219.46	125	[102, 103]	20220506D	0.3005	396.93	84.5	[83, 100]
20231011A	0.0783	186.3	70	[84, 101]	20230501A	0.3010	532.5	125.6	[100, 114]
20220509G	0.0894	269.53	55.2	[83]	20230503E	0.32	483.74	88	[118]
20230124	0.0940	590.6	38.5	[100]	20180924B	0.3214	361.42	40.5	[92, 113]

TABLE II: First part of the dataset of 131 localized FRBs reported by different radio telescopes.

FRB (name)	Redshift z	DM_{obs} (pc cm^{-3})	DM_{MW} (pc cm^{-3})	Ref.	FRB (name)	Redshift z	DM_{obs} (pc cm^{-3})	DM_{MW} (pc cm^{-3})	Ref.
20240310A	0.127	601.8	36	[86]	20230613A	0.3923	483.51	30	[118]
20210807D	0.1293	251.9	121	[86, 92]	20220204A	0.4	612.2	50.7	[99, 100, 114]
20240114A	0.13	527.7	49.7	[119]	20240208A	0.4	260.2	98	[86]
20240209A	0.1384	176.49	55.5	[120]	20230712A	0.4525	586.96	39.2	[99, 100, 114]
20210410D	0.1415	578.78	56.2	[92, 121]	20230907D	0.4638	1030.79	29	[118]
20230203A	0.1464	420.1	36.29	[84]	20181112A	0.4755	589.27	41.7	[92, 100]
20231226A	0.1569	329.9	145	[86]	20231020B	0.4775	952.2	34	[118]
20230526A	0.157	316.4	50	[86]	20220310F	0.479	462.15	46.3	[83, 100]
20220920A	0.158	314.99	40.3	[83]	20220918A	0.491	656.8	41	[86]
20200430A	0.1608	380.25	27	[113, 122]	20231210F	0.5	720.6	32	[118]
20230703A	0.1184	290.74	57.44	[84, 97]	20230902A	0.3619	440.1	34	[86]
20240213A	0.1185	357.4	40.1	[100]	20200906A	0.3688	577.84	35.8	[92, 122]
20240318A	0.12	256.4	37	[86]	20240119A	0.37	483.1	37.9	[100]
20230222A	0.1223	706.1	134.2	[84, 117]	20220330D	0.3714	468.1	38.6	[99, 100]
20190110C	0.1224	221.6	37.1	[88, 95]	20190611B	0.3778	322.2	57	[86, 92]
20230628A	0.1265	345.15	39.1	[99, 100, 114]	20220501C	0.381	449.5	31	[86]
20190711A	0.5217	587.9	56.4	[92, 100]	20190523A	0.6600	760.8	37.2	[100, 126]
20230216A	0.5310	828.0	38.5	[99, 100]	20220222C	0.853	1071.2	56	[118]
20230814B	0.5535	696.4	104.9	[100]	20240123A	0.968	1462.0	90.3	[100]
20221219A	0.5540	706.7	44.4	[99, 100, 114]	20221029A	0.9750	1391.05	43.9	[99, 100, 114]
20190614D	0.60	959.2	83.5	[122, 123]	20220610A	1.015	1458.1	30.9	[100, 127]
20231010A	0.61	442.59	41	[118]	20230521B	1.354	1342.9	138.8	[86, 100]
20220418A	0.6220	623.45	36.7	[83, 100]	20240304B	2.148	2458.2	28.1	[128]
20220224C	0.6271	1140.2	52	[118]	20230626A	0.3270	451.2	39.2	[99, 100, 114]
20231223C	0.1059	165.8	48	[84, 101]	20231025B	0.3238	368.7	48.59	[84, 117]
20201124A	0.098	413	123	[92, 124]	20230125D	0.3265	640.08	88	[118]
20230708A	0.105	411.51	50	[86]	20180301A	0.3304	536	151.6	[92, 100, 129]
20191106C	0.10775	333.2	25	[95]	20231220A	0.3355	491.2	49.9	[100]
20231128A	0.1079	331.6	25	[84, 101]	20211203C	0.3439	635.0	63.6	[92, 100]
20230222B	0.11	187.8	28	[84, 101]	20220208A	0.3510	437.0	101.6	[99, 100]
20231201A	0.1119	169.4	70	[84, 101]	20220726A	0.3610	686.55	89.5	[99, 100, 114]
20220914A	0.1139	631.28	55.2	[83]	20220717A	0.3630	637.34	118.33	[117, 130, 131]
20190608B	0.1178	338.7	33	[92, 122, 125]					

TABLE III: Second part of the dataset of 131 localized FRBs reported by different radio telescopes.

-
- [1] D. R. Lorimer, M. Bailes, M. A. McLaughlin, D. J. Narkevic, and F. Crawford, *Science* **318**, 777 (2007), arXiv:0709.4301 [astro-ph].
 - [2] J.-Y. Jia, D.-C. Qiang, L.-Y. Li, and H. Wei, Generalized distributions of host dispersion measures in the fast radio burst cosmology (2025), arXiv:2510.09463 [astro-ph.CO].
 - [3] T. Abbott et al. (The CHIME/FRB), *Astrophys. J. Suppl.* **283**, 34 (2026), arXiv:2601.09399 [astro-ph.HE].
 - [4] A. P. Curtin et al., *Astrophys. J.* **972**, 125 (2024), arXiv:2404.09242 [astro-ph.HE].
 - [5] A. P. Curtin et al., *Astrophys. J.* **992**, 206 (2025), arXiv:2411.02870 [astro-ph.HE].
 - [6] J. M. Cordes and I. Wasserman, *Mon. Not. Roy. Astron. Soc.* **457**, 232 (2016), arXiv:1501.00753 [astro-ph.HE].
 - [7] S. B. Popov and K. A. Postnov, (2007), arXiv:0710.2006 [astro-ph].

- [8] U.-L. Pen and L. Connor, *Astrophys. J.* **807**, 179 (2015), arXiv:1501.01341 [astro-ph.HE].
- [9] M. A. Abramowicz, M. Bejger, and M. Wielgus, *Astrophys. J.* **868**, 17 (2018), arXiv:1704.05931 [astro-ph.HE].
- [10] G. M. Fuller, A. Kusenko, and V. Takhistov, *Phys. Rev. Lett.* **119**, 061101 (2017), arXiv:1704.01129 [astro-ph.HE].
- [11] K. Kainulainen, S. Nurmi, E. D. Schiappacasse, and T. T. Yanagida, *Phys. Rev. D* **104**, 123033 (2021), arXiv:2108.08717 [astro-ph.HE].
- [12] D. W. P. Amaral and E. D. Schiappacasse, *Phys. Rev. D* **110**, 083532 (2024), arXiv:2312.09285 [hep-ph].
- [13] B. Carr, S. Clesse, J. Garcia-Bellido, M. Hawkins, and F. Kuhnel, *Phys. Rept.* **1054**, 1 (2024), arXiv:2306.03903 [astro-ph.CO].
- [14] C.-M. Deng, Y. Cai, X.-F. Wu, and E.-W. Liang, *Phys. Rev. D* **98**, 123016 (2018), arXiv:1812.00113 [astro-ph.HE].
- [15] M. Meng, Q.-J. Huang, and C.-M. Deng, *Res. Astron. Astrophys.* **24**, 095006 (2024).
- [16] S. Kalita, S. Bhatporia, and A. Weltman, *Phys. Dark Univ.* **48**, 101926 (2025), arXiv:2410.01974 [astro-ph.CO].
- [17] J. B. Muñoz and A. Loeb, *Phys. Rev. D* **98**, 103518 (2018), arXiv:1809.04074 [astro-ph.CO].
- [18] A. Walters, Y.-Z. Ma, J. Sievers, and A. Weltman, *Phys. Rev. D* **100**, 103519 (2019), arXiv:1909.02821 [astro-ph.CO].
- [19] D.-C. Qiang and H. Wei, *JCAP* **04**, 023, arXiv:2002.10189 [astro-ph.CO].
- [20] J. B. Muñoz, E. D. Kovetz, L. Dai, and M. Kamionkowski, *Physical Review Letters* **117**, 10.1103/physrevlett.117.091301 (2016).
- [21] T. D. Brandt, *Astrophys. J. Lett.* **824**, L31 (2016), arXiv:1605.03665 [astro-ph.GA].
- [22] Y. K. Wang and F. Y. Wang, *Astron. Astrophys.* **614**, A50 (2018), arXiv:1801.07360 [astro-ph.CO].
- [23] C. Leung *et al.*, *Phys. Rev. D* **106**, 043017 (2022), arXiv:2204.06001 [astro-ph.HE].
- [24] S. Kalita, S. Bhatporia, and A. Weltman, *JCAP* **11**, 059, arXiv:2308.16604 [gr-qc].
- [25] S. Profumo, *JCAP* **10**, 075, arXiv:2508.06688 [astro-ph.HE].
- [26] J.-H. Li, S.-J. Wang, X.-Y. Zhao, and N. Li, *Universe* **11**, 311 (2025).
- [27] Y. B. Zel'dovich and I. D. Novikov, *Sov. Astron.* **10**, 602 (1967).
- [28] S. Hawking, *Mon. Not. Roy. Astron. Soc.* **152**, 75 (1971).
- [29] B. J. Carr and S. W. Hawking, *Mon. Not. Roy. Astron. Soc.* **168**, 399 (1974).
- [30] B. Carr and F. Kuhnel, *Ann. Rev. Nucl. Part. Sci.* **70**, 355 (2020), arXiv:2006.02838 [astro-ph.CO].
- [31] P. Mroz *et al.*, *Nature* **548**, 183 (2017), arXiv:1707.07634 [astro-ph.EP].
- [32] H. Niihara, M. Takada, S. Yokoyama, T. Sumi, and S. Masaki, *Phys. Rev. D* **99**, 083503 (2019), arXiv:1901.07120 [astro-ph.CO].
- [33] S. Sugiyama, M. Takada, N. Yasuda, and N. Tominaga, (2026), arXiv:2602.05840 [astro-ph.CO].
- [34] G. Hütsi, M. Raidal, V. Vaskonen, and H. Veermäe, *JCAP* **03**, 068, arXiv:2012.02786 [astro-ph.CO].
- [35] E. Berti, F. Crescimbeni, G. Franciolini, S. Mastrogiovanni, P. Pani, and G. Pierra, *Phys. Rev. D* **113**, 043048 (2026), arXiv:2512.03152 [gr-qc].
- [36] M. Kawasaki, A. Kusenko, and T. T. Yanagida, *Phys. Lett. B* **711**, 1 (2012), arXiv:1202.3848 [astro-ph.CO].
- [37] J. L. Bernal, A. Raccanelli, L. Verde, and J. Silk, *JCAP* **05**, 017, [Erratum: *JCAP* 01, E01 (2020)], arXiv:1712.01311 [astro-ph.CO].
- [38] C. T. Byrnes, J. Lesgourgues, and D. Sharma, *JCAP* **09**, 012, arXiv:2404.18475 [astro-ph.CO].
- [39] M. Sasaki, T. Suyama, T. Tanaka, and S. Yokoyama, *Class. Quant. Grav.* **35**, 063001 (2018), arXiv:1801.05235 [astro-ph.CO].
- [40] A. M. Green and B. J. Kavanagh, *J. Phys. G* **48**, 043001 (2021), arXiv:2007.10722 [astro-ph.CO].
- [41] C. Casanueva-Villarreal, N. Padilla, P. B. Tissera, B. Liu, and V. Bromm, *Astron. Astrophys.* **699**, A49 (2025), arXiv:2505.10706 [astro-ph.CO].

- [42] C. Byrnes, G. Franciolini, T. Harada, P. Pani, and M. Sasaki, eds., *Primordial Black Holes*, Springer Series in Astrophysics and Cosmology (Springer, 2025).
- [43] M. Zumalacarregui and U. Seljak, *Phys. Rev. Lett.* **121**, 141101 (2018), arXiv:1712.02240 [astro-ph.CO].
- [44] P. Mróz *et al.*, *Nature* **632**, 749 (2024), arXiv:2403.02386 [astro-ph.GA].
- [45] P. Mróz *et al.*, *Astrophys. J. Suppl.* **280**, 49 (2025), arXiv:2507.13794 [astro-ph.GA].
- [46] M. Oguri, J. M. Diego, N. Kaiser, P. L. Kelly, and T. Broadhurst, *Phys. Rev. D* **97**, 023518 (2018), arXiv:1710.00148 [astro-ph.CO].
- [47] M. Andrés-Carcasona, A. J. Iovino, V. Vaskonen, H. Veermäe, M. Martínez, O. Pujolàs, and L. M. Mir, *Phys. Rev. D* **110**, 023040 (2024), arXiv:2405.05732 [astro-ph.CO].
- [48] P. D. Serpico, V. Poulin, D. Inman, and K. Kohri, *Phys. Rev. Res.* **2**, 023204 (2020), arXiv:2002.10771 [astro-ph.CO].
- [49] D. Agius, R. Essig, D. Gaggero, F. Scarcella, G. Suczewski, and M. Valli, *JCAP* **07**, 003, arXiv:2403.18895 [hep-ph].
- [50] B. Carr, K. Kohri, Y. Sendouda, and J. Yokoyama, *Rept. Prog. Phys.* **84**, 116902 (2021), arXiv:2002.12778 [astro-ph.CO].
- [51] B. Carr, A. J. Iovino, G. Perna, V. Vaskonen, and H. Veermäe 10.1007/s40766-026-00080-z (2026), arXiv:2601.06024 [astro-ph.CO].
- [52] LOFAR, LOFAR2.0 White paper, <https://www.lofar.eu/lofar2-0-documentation/> (2023), [Online; accessed 17-April-2026].
- [53] J. Wang, M. J. Norden, and P. Donker, (2025), arXiv:2503.02425 [astro-ph.IM].
- [54] T. W. Shimwell *et al.*, *Astron. Astrophys.* **707**, A198 (2026), arXiv:2602.15949 [astro-ph.GA].
- [55] P. Jiang, R. Chen, H. Gan, J. Sun, B. Zhu, H. Li, W. Zhu, J. Wu, X. Chen, H. Zhang, and T. An, *Astronomical Techniques and Instruments* **1**, 84 (2024), arXiv:2408.12826 [astro-ph.IM].
- [56] E. Abdalla *et al.*, *Astron. Astrophys.* **664**, A14 (2022), arXiv:2107.01633 [astro-ph.CO].
- [57] M. V. dos Santos *et al.*, *Astron. Astrophys.* **681**, A120 (2024), arXiv:2308.06805 [astro-ph.IM].
- [58] E. Abdalla *et al.* (2023) arXiv:2309.05099 [astro-ph.CO].
- [59] N. Aghanim *et al.* (Planck), *Astron. Astrophys.* **641**, A6 (2020), [Erratum: *Astron. Astrophys.* 652, C4 (2021)], arXiv:1807.06209 [astro-ph.CO].
- [60] E. Petroff *et al.*, *Mon. Not. Roy. Astron. Soc.* **447**, 246 (2015), arXiv:1412.0342 [astro-ph.HE].
- [61] C. W. James, J. X. Prochaska, J.-P. Macquart, F. O. North-Hickey, K. W. Bannister, and A. Dunning, *Monthly Notices of the Royal Astronomical Society* **509**, 4775–4802 (2021).
- [62] J. P. Macquart *et al.*, *Nature* **581**, 391 (2020), arXiv:2005.13161 [astro-ph.CO].
- [63] J. M. Shull, B. D. Smith, and C. W. Danforth, *The Astrophysical Journal* **759**, 23 (2012).
- [64] A. A. Meiksin, *Rev. Mod. Phys.* **81**, 1405 (2009), arXiv:0711.3358 [astro-ph].
- [65] G. D. Becker, J. S. Bolton, M. G. Haehnelt, and W. L. W. Sargent, *Mon. Not. Roy. Astron. Soc.* **410**, 1096 (2011), arXiv:1008.2622 [astro-ph.CO].
- [66] M. Bartelmann, *Class. Quant. Grav.* **27**, 233001 (2010), arXiv:1010.3829 [astro-ph.CO].
- [67] M. W. Sammons, J.-P. Macquart, R. D. Ekers, R. M. Shannon, H. Cho, J. X. Prochaska, A. T. Deller, and C. K. Day, *Astrophys. J.* **900**, 122 (2020), arXiv:2002.12533 [astro-ph.CO].
- [68] L. L. Sales, K. E. L. de Farias, A. R. Queiroz, J. R. L. Santos, R. A. Batista, A. R. M. Oliveira, L. F. Santana, C. A. Wuensche, T. Villela, and J. Vieira, (2025), arXiv:2507.06975 [astro-ph.CO].
- [69] M. P. van Haarlem *et al.* (LOFAR), *Astron. Astrophys.* **556**, A2 (2013), arXiv:1305.3550 [astro-ph.IM].
- [70] P. Chawla, A. Gopinath, N. Manaswini, C. Bassa, J. Hessels, V. Kondratiev, D. Michilli, and Z. Pleunis, *Mon. Not. Roy. Astron. Soc.* **544**, 4079 (2025), arXiv:2509.01688 [astro-ph.HE].
- [71] X. X. Zhang, R. Duan, V. Gajjar, H. Y. Zhang, P. Wang, C. H. Niu, D. Werthimer, J. Cobb, S. Y. Li, X. Pei, Y. Zhu, and D. Li, *Research in Astronomy and Astrophysics* **23**, 095023 (2023).
- [72] C. A. Wuensche *et al.*, *Astron. Astrophys.* **664**, A15 (2022), arXiv:2107.01634 [astro-ph.IM].
- [73] S. Sanidas *et al.*, *Astron. Astrophys.* **626**, A104 (2019), arXiv:1905.04977 [astro-ph.HE].
- [74] S. K. Acharya and P. Beniamini, (2025), arXiv:2503.08441 [astro-ph.CO].

- [75] X. Pritchard, C. T. Byrnes, J. Lesgourgues, and D. Sharma, *JCAP* **07**, 079, arXiv:2505.08442 [astro-ph.CO].
- [76] H. Niikura *et al.*, *Nature Astron.* **3**, 524 (2019), arXiv:1701.02151 [astro-ph.CO].
- [77] A. H. Nitz and Y.-F. Wang, *Phys. Rev. D* **106**, 023024 (2022), arXiv:2202.11024 [astro-ph.HE].
- [78] P. Mróz *et al.*, *Astrophys. J. Suppl.* **273**, 4 (2024), arXiv:2403.02398 [astro-ph.GA].
- [79] B. J. Kavanagh, D. Gaggero, and G. Bertone, *Phys. Rev. D* **98**, 023536 (2018), arXiv:1805.09034 [astro-ph.CO].
- [80] B. J. Kavanagh, *Pbhounds* (2019).
- [81] T. C. Abbott *et al.* (CHIME, FRB), *Astrophys. J. Lett.* **989**, L48 (2025), arXiv:2506.19006 [astro-ph.HE].
- [82] E. K. Mahony *et al.*, *Astrophys. J. Lett.* **867**, L10 (2018), arXiv:1810.04354 [astro-ph.HE].
- [83] C. J. Law *et al.*, *Astrophys. J.* **967**, 29 (2024), arXiv:2307.03344 [astro-ph.HE].
- [84] M. Amiri *et al.* (CHIME/FRB), *Astrophys. J. Suppl.* **280**, 6 (2025), arXiv:2502.11217 [astro-ph.HE].
- [85] S. Feng, Y. Gong, X. Liu, J.-H. Yan, and X. Chen, *Astrophys. J.* **1000**, 146 (2026), arXiv:2510.23105 [astro-ph.CO].
- [86] R. M. Shannon *et al.*, *Publ. Astron. Soc. Austral.* **42**, e036 (2025), arXiv:2408.02083 [astro-ph.HE].
- [87] M. Bhardwaj *et al.*, *Astrophys. J. Lett.* **971**, L51 (2024), arXiv:2310.10018 [astro-ph.HE].
- [88] M. Amiri *et al.* (CHIME/FRB), *Astrophys. J. Suppl.* **257**, 59 (2021), arXiv:2106.04352 [astro-ph.HE].
- [89] R. N. Li, K. Xu, D. H. Gao, Q. Wu, S. X. Yi, and F. Y. Wang, *The Astrophysical Journal* **989**, 77 (2025).
- [90] M. Bhardwaj *et al.*, *Astrophys. J. Lett.* **910**, L18 (2021), arXiv:2103.01295 [astro-ph.HE].
- [91] M. Bhardwaj *et al.*, *Astrophys. J. Lett.* **919**, L24 (2021), arXiv:2108.12122 [astro-ph.HE].
- [92] A. C. Gordon *et al.*, *Astrophys. J.* **954**, 80 (2023), arXiv:2302.05465 [astro-ph.GA].
- [93] M. Glowacki, A. Bera, K. Lee-Waddell, A. Deller, T. Dial, K. Gourdji, S. Simha, M. Caleb, L. Marnoch, J. X. Prochaska, *et al.*, *The Astrophysical Journal Letters* **962**, L13 (2024).
- [94] K. M. Rajwade *et al.*, *Mon. Not. Roy. Astron. Soc.* **514**, 1961 (2022), arXiv:2205.14600 [astro-ph.HE].
- [95] A. L. Ibik *et al.*, *Astrophys. J.* **961**, 99 (2024), arXiv:2304.02638 [astro-ph.HE].
- [96] D. Michilli *et al.*, *Astrophys. J.* **950**, 134 (2023), arXiv:2212.11941 [astro-ph.HE].
- [97] A. E. Lanman, S. Simha, *et al.*, arXiv e-prints, arXiv:2509.07097 (2025), arXiv:2509.07097 [astro-ph.GA].
- [98] L. N. Driessen *et al.*, *Mon. Not. Roy. Astron. Soc.* **527**, 3659 (2023), arXiv:2302.09787 [astro-ph.HE].
- [99] K. Sharma *et al.*, *Nature* **635**, 61 (2024), arXiv:2409.16964 [astro-ph.HE].
- [100] L. Connor *et al.*, *Nature Astron.* **9**, 1226 (2025), arXiv:2409.16952 [astro-ph.CO].
- [101] C. Leung *et al.* (CHIME/FRB), *Astrophys. J. Lett.* **991**, L25 (2025), arXiv:2507.16816 [astro-ph.GA].
- [102] V. Ravi *et al.* (Deep Synoptic Array Team), *Astrophys. J. Lett.* **949**, L3 (2023), arXiv:2211.09049 [astro-ph.HE].
- [103] Y.-K. Zhang *et al.*, *Astrophys. J.* **955**, 142 (2023), arXiv:2304.14665 [astro-ph.HE].
- [104] A. P. Curtin *et al.*, *Astrophys. J.* **998**, 97 (2026), arXiv:2506.10961 [astro-ph.HE].
- [105] T. Cassanelli *et al.*, *Nature Astron.* **8**, 1429 (2024), arXiv:2307.09502 [astro-ph.HE].
- [106] D. H. Gao, Q. Wu, J. P. Hu, S. X. Yi, X. Zhou, F. Y. Wang, and Z. G. Dai, *Astron. Astrophys.* **698**, A215 (2025), arXiv:2410.03994 [astro-ph.CO].
- [107] Y. Li *et al.*, *Science* **391**, 280 (2026), arXiv:2503.04727 [astro-ph.HE].
- [108] J.-G. Zhang, J.-Y. Song, W.-P. Sun, Z.-W. Zhao, J.-F. Zhang, and X. Zhang, (2025), arXiv:2507.06841 [astro-ph.CO].
- [109] M. P. Snelders *et al.*, (2025), arXiv:2510.11352 [astro-ph.HE].
- [110] S. Bhandari *et al.*, *Astrophys. J.* **948**, 67 (2023), arXiv:2211.16790 [astro-ph.HE].
- [111] S. Bhandari *et al.*, *Astrophys. J. Lett.* **901**, L20 (2020), arXiv:2008.12488 [astro-ph.HE].
- [112] M. Hussaini, L. Connor, R. M. Konietzka, V. Ravi, J. Faber, K. Sharma, and M. Sherman, *Astrophys. J. Lett.* **993**, L27 (2025), arXiv:2506.04186 [astro-ph.CO].
- [113] J.-J. Wei and F. Melia, *Astrophys. J.* **955**, 101 (2023), arXiv:2308.05918 [astro-ph.CO].

- [114] M. B. Sherman et al. (Deep Synoptic Array Team), *Astrophys. J.* **964**, 131 (2024), arXiv:2308.06813 [astro-ph.HE].
- [115] S. Koch Ocker, J. M. Cordes, S. Chatterjee, C.-H. Niu, D. Li, J. W. McKee, C. J. Law, C.-W. Tsai, R. Anna-Thomas, J.-M. Yao, and M. Cruces, *The Astrophysical Journal* **931**, 87 (2022).
- [116] S. Bhandari et al., *Astron. J.* **163**, 69 (2022), arXiv:2108.01282 [astro-ph.HE].
- [117] J. Zhuge, M. Kalomenopoulos, and B. Zhang, *Astrophys. J.* **996**, 66 (2026), arXiv:2508.05161 [astro-ph.CO].
- [118] I. Pastor-Marazuela et al., *Mon. Not. Roy. Astron. Soc.* **545**, staf2144 (2026), arXiv:2507.05982 [astro-ph.HE].
- [119] A. Kumar, Y. Maan, and Y. Bhusare, *Astrophys. J.* **977**, 177 (2024), arXiv:2406.12804 [astro-ph.HE].
- [120] V. Shah et al., *Astrophys. J. Lett.* **979**, L21 (2025), arXiv:2410.23374 [astro-ph.HE].
- [121] M. Caleb et al., *Mon. Not. Roy. Astron. Soc.* **524**, 2064 (2023), arXiv:2302.09754 [astro-ph.HE].
- [122] D. Hiramatsu, E. Berger, B. D. Metzger, S. Gomez, A. Bieryla, I. Arcavi, D. A. Howell, R. Mckinven, and N. Tominaga, *Astrophys. J. Lett.* **947**, L28 (2023), arXiv:2211.03974 [astro-ph.HE].
- [123] C. J. Law et al., *Astrophys. J.* **899**, 161 (2020), arXiv:2007.02155 [astro-ph.HE].
- [124] A. E. Lanman et al., *Astrophys. J.* **927**, 59 (2022), arXiv:2109.09254 [astro-ph.HE].
- [125] J. S. Chittidi, S. Simha, et al., *Astrophys. J.* **922**, 173 (2021), arXiv:2005.13158 [astro-ph.GA].
- [126] V. Ravi et al., *Nature* **572**, 352 (2019), arXiv:1907.01542 [astro-ph.HE].
- [127] S. D. Ryder et al., *Science* **392**, 294 (2023), arXiv:2210.04680 [astro-ph.HE].
- [128] M. Caleb et al., (2025), arXiv:2508.01648 [astro-ph.HE].
- [129] D. C. Price et al., *Mon. Not. Roy. Astron. Soc.* **486**, 3636 (2019), arXiv:1901.07412 [astro-ph.HE].
- [130] K. M. Rajwade et al., *Mon. Not. Roy. Astron. Soc.* **532**, 3881 (2024), arXiv:2407.02173 [astro-ph.HE].
- [131] C. Xu, Y. Feng, and J. Xu, *The Astrophysical Journal* **988**, 177 (2025).